

pubs.acs.org/journal/abseba Article

Membrane-Wrapped Nanoparticles for Enhanced Chemotherapy of Acute Myeloid Leukemia

Jenna C. Harris, Eric H. Sterin, and Emily S. Day*



Cite This: https://doi.org/10.1021/acsbiomaterials.2c00832



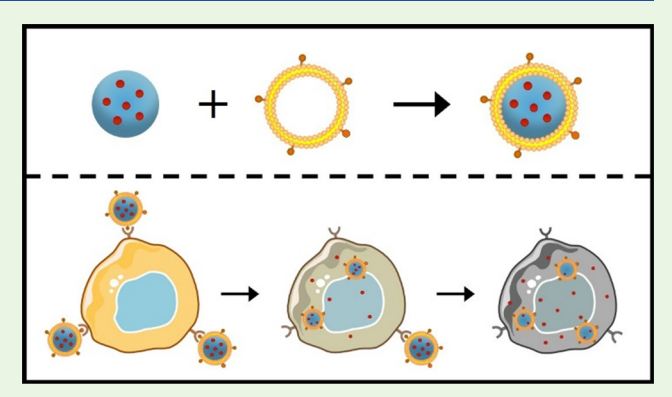
ACCESS

III Metrics & More

Article Recommendations

Supporting Information

ABSTRACT: This work reports the development of a biomimetic membrane-wrapped nanoparticle (MWNP) platform for targeted chemotherapy of acute myeloid leukemia (AML). Doxorubicin (DOX), a chemotherapeutic used to treat leukemias, lymphomas, and other cancers, was encapsulated in polymeric NPs that were coated with cytoplasmic membranes derived from human AML cells. The release rate of DOX from the MWNPs was characterized under both storage and physiological conditions, with faster release observed at pH 5.5 than pH 7.4. The system was then introduced to AML cell cultures to test the functionality of the released DOX cargo as compared to DOX delivered freely or *via* NPs coated with poly(ethylene glycol) (PEG). The MWNPs delivered DOX in an efficient and targeted manner, inducing up to 80% apoptosis in treated cells at a dose of 5 μ M, compared to 15% for free DOX and



17% for DOX-loaded PEG-coated NPs at the same drug concentration. The mechanism of cell death was confirmed as DNA double-strand breaks through a γ H2A.X assay, indicating that the released DOX retained its expected mechanism of action. These findings designate MWNPs as a robust drug delivery system with great potential for future development in treatments of AML and other blood cancers.

KEYWORDS: biomimetic, membrane-coated, biomimicry, cancer, doxorubicin, drug release

1. INTRODUCTION

Acute myeloid leukemia (AML) is a bone marrow disorder wherein hematopoietic stem and progenitor cells (HSPCs) are genetically altered, leading to an expansion in immature myeloid cells and a reduction in healthy HSPCs. ^{1,2} As HSPCs are multipotent cells that can differentiate into all blood cell types, their reduction and failure have adverse effects throughout the body. Currently, harsh treatment regimens are applied in attempt to eradicate all cancerous cells in the body. This has increased the five-year survival rate for younger patients with AML over the decades, from 13% in the 1970s to 55% in the 2010s, but the survival rate for patients over 60 remains below 20%. Developing more effective and patient-friendly treatments for AML and other HSPC disorders is of great importance.

Traditional treatment for AML begins with induction chemotherapy where a cytarabine-based drug is given over the course of 7 days and an anthracycline-based drug is overlapped for the first 3 days of treatment. The goal of this intensive treatment is to clear the body of leukemia cells and reduce the quantity of cancerous bone marrow cells, enabling the cancer to be contained within a few rounds of induction chemotherapy. If AML is absent after this step, then consolidation chemotherapy begins. Here, patients are subject

to regular injections of chemotherapy over the course of several months to ensure that all the leukemia cells have been killed. If the outcome of induction therapy was not as positive, then patients, especially those who are younger and stronger, are then prepared for a bone marrow transplant through more chemotherapy. Unfortunately, the amount of chemotherapy required for AML management is extremely taxing for patients regardless of which treatment path they are on. As alternatives to these traditional treatment plans, new targeted treatments have started to enter the market, including antibody-drug conjugates. One targets CD33+ AML cells for delivery of calicheamicin, a cytotoxic agent that induces DNA damage. 8,9 However, there are drawbacks to this system including rapid clearance, inconsistent drug-to-antibody ratios, and unconjugated antibodies providing no therapeutic advantage.5 Further, CD33 is sporadically expressed on AML cells, which

Received: July 20, 2022 Accepted: September 2, 2022



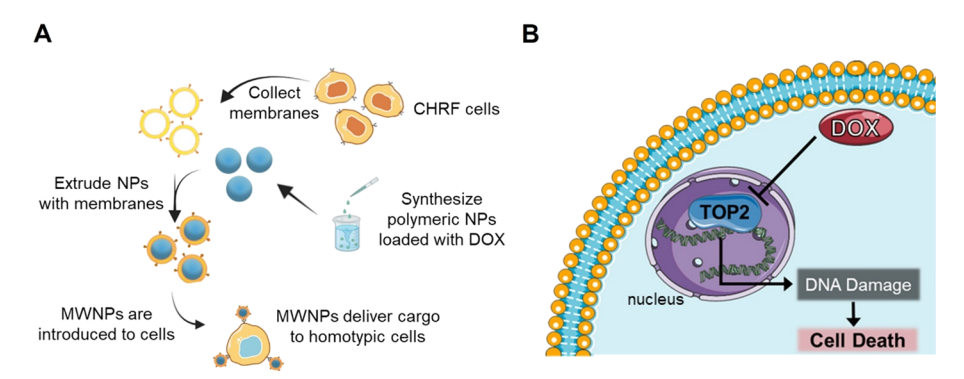


Figure 1. Overview of the synthesis, application, and intracellular activity of MWNPs. (A) DOX-loaded NPs are wrapped in membranes extracted from CHRF-288-11 cells, a childhood acute megakaryoblastic leukemia cell line, to enable homotypic targeting to AML cells. (B) Once inside the cell, DOX blocks topoisomerase-II, causing DNA damage, resulting in cell death. Parts of the figure were produced using Servier Medical Art templates. Servier Medical Art by Servier is licensed under a Creative Commons Attribution 3.0 Unported License (https://creativecommons.org/licenses/by/3.0/).

leaves a population of untargeted cells capable of inducing relapse.

While the importance of targeted therapies and singlemolecule inhibitors for the treatment of leukemia and other HSPC disorders cannot be discounted, their insufficient efficacy may be attributed to a mismatch between heterogeneous cell receptor expression and the single-targeting moiety used in such formulations. One approach to tackle this problem was to utilize liquid nitrogen-treated AML cells to deliver doxorubicin (DOX) to the bone marrow. 10 By cryoshocking the cancer cells, the bone marrow targeting capabilities were maintained, while the pathogenic properties of the cells were removed. The delivery of DOX via this system was less effective than free DOX in vitro but allowed for longer circulation and increased bone marrow accumulation in vivo. 10 To allow for more tunability, we have developed an effective, nanoparticle-based, drug delivery system that uses the diverse array of cell-specific binding proteins present on cell membranes to engage the multiple receptors present on target cells. Membrane-wrapped nanoparticles (MWNPs) have shown great promise as a targeted drug delivery system for a variety of cancers. 11-14 Specifically regarding MWNPs for AML, scientists have explored using mouse-derived AML cell membranes as a coating to wrap poly(lactic-co-glycolic acid) (PLGA) NPs loaded with CpG adjuvant for immunotherapy and cancer vaccination. 15 This system showed promise in both prophylactic and post-remission vaccination models. ¹⁵ In this work, polymeric NPs were loaded with the chemotherapeutic doxorubicin and coated with cytoplasmic membranes derived from human CHRF-288-11 (CHRF) cells, which were originally isolated from an infant with acute megakaryoblastic leukemia. These AML MWNPs deliver their cargo efficiently to targeted AML cells and induce apoptosis at up to 5× higher rates than their free drug or untargeted counterparts. The potential application of these MWNPs for AML treatment is depicted in Figure 1A.

Doxorubicin (DOX), clinically known as adriamycin, was selected as the drug cargo because it has been used to treat leukemias, lymphomas, and other cancers, usually in combination with a cytarabine. Anthracyclines like DOX inhibit the functionality of the enzyme topoisomerase-II (TOP2), resulting in DNA damage and apoptotic cell death (Figure 1B). This DNA breakage is marked by the highly specific and sensitive event of the phosphorylation of histone

H2AX at the serine-139 residue, resulting in γ H2AX.²¹ While most commonly cited, this is not the only mechanism by which DOX induces cell death. Intracellular reduction of DOX can rupture the mitochondrial membrane through formation of reactive oxygen species (ROS), and DOX can also bind with ferritin, affecting the intracellular iron concentration. ^{22–25} This iron binding is of specific concern in cardiomyocytes as a major drawback of DOX is the cardiotoxicity caused by repeat dosing, suspected to be due to the upregulation of death receptors. ^{19,23,26} While modifying the dosing regimen may be a feasible strategy to limit cardiotoxicity, an alternative approach to increase efficacy and safety would be to deliver DOX in a targeted carrier system like MWNPs that minimizes accumulation in cardiomyocytes and enhances accumulation in targeted cancer cells. ¹⁹

Delivering chemotherapeutic cargo to the bone marrow through homotypic targeting may be enough of a breakthrough as targeted, non-systemic delivery would be advantageous to the patient. However, previous data has shown that Mk-based delivery systems are not only able to target bone marrow but also specifically reach CD117+ cells.²⁷ Work by Escobar et al. showed that human Mk microparticles reached CD117+ cells at higher levels than cells expressing two other tested membrane markers (CD41 and CD45).²⁷ In the work presented here, CHRF membranes were used as they are both an acute megakaryoblastic leukemia cell line and a previously established Mk model.^{28,29} By stimulating CHRF cells with phorbol 12-myrsitate 13-acetate (PMA), they follow the differentiation pathway of the early Mk phenotype to primary Mk, expressing a similar genetic pattern to Mk cells.²⁸ Kao and Papoutsakis demonstrated that CHRF-derived microparticles performed as well as Mk microparticles in targeting HSPCs, with 98.1% of the CHRF microparticles being recognized and taken up by HSPCs, compared to 98.9% of the Mk microparticles.²⁹ Based on these studies, we postulated that CHRF MWNPs would be similar to Mk microparticles and CHRF microparticles in their ability to target CD117+ cells at higher levels than non-targeted counterparts. CD117, or c-Kit, is a transmembrane receptor present on HSPCs, erythroid, myeloid, and megakaryocytic precursors as well as up to 87% of AML cell lines.^{30–34} It is one of the "most promising target antigens" for treatment of AML and other HSPC disorders. 16 By specifically reaching CD117+ cells, MWNPs would be able to avoid downstream, differentiated, healthy bone marrow cells, limiting side effects and making recovery from chemotherapy and preparation for bone marrow transplants a less taxing process.³⁵ Stated another way, this system has great potential to improve patient quality of life during treatment upon further development, validation, and implementation.

In this work, we demonstrate the synthesis of DOX-loaded, CHRF membrane-wrapped polymer NPs and evaluate their effects on AML cells *in vitro*. A 5 μ M dose of AML MWNPs yields apoptosis in approximately 80% of treated AML cells, compared to 16.5 and 14.9% for untargeted DOX-loaded NPs and free DOX, respectively. This corresponds to a remarkable 5× improved efficacy of the drug through its loading in MWNPs. Further analysis of γ H2AX confirmed that the DOX-MWNPs induce DNA damage as expected. These exciting results support continued development of MWNPs for targeted chemotherapy of AML.

2. EXPERIMENTAL SECTION

2.1. Cell Culture and Membrane Collection. CHRF-288-11 cells were used for all experiments. CHRF cells are a childhood acute megakaryoblastic leukemia cell line that differentiates into Mk-like cells after treatment with phorbol 12-myrsitate 13-acetate (PMA). ^{28,29} Cells were grown in 300 cm² cell culture-treated flasks in Iscove's modified Dulbecco's medium supplemented with 10% fetal bovine serum (FBS), 3.02 g/L sodium bicarbonate, and 1% antibiotic—antimycotic (Gibco). To induce Mk-like characteristics, CHRF cells were seeded in the same type of flask at 500,000 cells/mL and treated with 10 ng/mL PMA. After 24–48 h of incubation, the CHRF cells were either used for *in vitro* experiments or for collection of membrane vesicles.

Membrane vesicles were prepared from PMA-treated CHRF cells through a lysis and centrifugation process adapted from Fang et al.³⁶ Briefly, media were centrifuged at 300g to collect any non-adherent cells and 8 mL of 0.25% trypsin-EDTA (ThermoFisher) was added to detach adherent cells. After detaching, the media were added to neutralize trypsin and cells were pelleted by centrifugation at 300g. After pelleting, all cells were washed 3 times with cold phosphatebuffered saline (PBS) and suspended in a hypotonic lysis buffer (20 mM Tris HCl, 10 mM KCl, and 2 mM MgCl2) with 1× protease inhibitor (ThermoFisher). The solution was then emulsified using a Dounce homogenizer (Kimble) with two different size pestles. The mixture was then centrifuged at 3200g for 5 min at 4 °C. The supernatant was collected, and the pellet was subjected to the homogenization and centrifuge steps again. The nuclear pellet formed from this step was discarded, and the combined supernatants were then centrifuged at 20,000g for 20 min at 4 °C. This mitochondrial pellet was discarded, and the supernatant was centrifuged at 100,000g for 90 min at 4 °C, pelleting the membranes. The final pellet was resuspended in water and extruded through a 400 nm polycarbonate membrane using a mini extruder (Avanti) at 75 °C to create monodisperse membrane vesicles.

2.2. Synthesis of DOX-Loaded PEG-PLGA NPs. DOX-loaded poly(ethylene glycol)-poly(lactic-co-glycolic acid) (PEG-PLGA) NPs were synthesized using methods for single emulsion NPs adapted from the literature. $^{37-39}$ PLGA (39.5 kDa, 50:50 carboxylic acid terminated, LACTEL Absorbable Polymers) was dissolved in acetone at 2 mg/mL. Separately, methoxy-PEG(5 kDa)-PLGA(30 kDa) (NanoSoft Polymers, 50:50) was dissolved in dichloromethane (DCM) at 2 mg/mL and then mixed with the acetone-PLGA solution at a 1:3 ratio with the total volume equaling 1 mL. 40 Next, 50 μ g of DOX hydrochloride (Sigma) at a concentration of 25 μ g/ μ L was added to the mixture and the solution was added dropwise to 3 mL of 0.1% poly(vinyl alcohol) (Sigma) in water and probe sonicated on ice with a Fisherbrand model 120 Sonic Dismembrator (Fisher Scientific) at 80% amplitude for 60 s. The solvent was allowed to evaporate overnight at room temperature in a fume hood under continuous stirring at 800 rpm, and the DOX-loaded PEG-PLGA NPs

were purified by 50 kDa molecular weight cutoff (MWCO) centrifugal filtration (Sigma) at 3200g for 20 min at 4 $^{\circ}$ C to remove unencapsulated DOX and excess solvent. NPs were left unwrapped to prepare PEG-PLGA control particles or wrapped with CHRF membranes as described below to produce MWNPs.

2.3. Synthesis of Membrane-Wrapped NPs (MWNPs). The concentrations of CHRF membrane vesicles and purified DOXloaded PEG-PLGA NPs were measured by nanoparticle tracking analysis (NTA, NanoSight NS300). Beyond concentration, NTA can also determine the diameter of particles through light scattering and Brownian motion, correlating the particle motion to size. Samples were diluted in 1 mL of water to a particle count between 20 and 100 particles per frame, and the concentration and size were calculated from data collected during three 30 s videos. Once concentrations were determined via NTA, membranes and NPs were mixed at a 2:1 numeric ratio and co-extruded through a 400 nm polycarbonate membrane (Avanti) for seven passes in a heating block at 75 °C to create MWNPs. MWNPs were centrifuged at 20,000g for 20 min at 4 °C to pellet the NP fraction, and the supernatant was discarded. The pellet containing MWNPs was resuspended in water for further experimental use. MWNPs were not further purified, and it was assumed that a majority of NPs were wrapped based on the excess of membranes used when extruding, though this was not experimentally validated. Particles were used fresh (within 2 h of synthesis).

2.4. Characterization of NPs and Encapsulation of DOX. The size and concentration of PEG-PLGA NPs, CHRF membranes, and MWNPs were measured by NTA. For this, 1-5 μ L of sample was diluted in water to a total volume of 1 mL. Particle count per frame was typically between 20 and 100, and the camera level was adjusted until particles were visible, but fewer than 20% had signal saturation. The focus was modified for each sample until particles were clear and visible with few double rings. After completing three 30 s videos at a syringe speed of 50-60 A.U. with the syringe pump, the detection threshold was set so the blue cross count was less than four for each frame.⁴¹ From the analysis of these three videos, the concentration, mode size, and mean size were obtained. The zeta potential was determined using an Anton Paar LiteSizer500 instrument. Samples were diluted in water and added to omega cuvettes where the reported values were the triplicate average of 200 runs. Morphology was confirmed by transmission electron microscopy (TEM) where samples were prepared on 400 nm mesh carbon-coated grids. Grids were treated by a PELCO easiGlow glow discharge cleaning system to allow for easy sample adherence, and samples were stained with 2% uranyl acetate. Samples were imaged using a Zeiss LIBRA 120 TEM.

To further verify that the membrane coating present on the particles consisted of only the extracellular components and that the intracellular components were removed during the membrane collection process, sodium dodecyl-sulfate polyacrylamide gel electrophoresis (SDS-PAGE) was performed. Protein content of homogenized cells, nuclear pellet, mitochondrial pellet, membrane vesicles, and MWNPs was measured by detergent compatible (DC) protein assay (Bio-Rad) following manufacturer's protocols. Subsequently, 20 $\mu {\rm g}$ of protein was loaded into a Bolt 4–12% Bis-Tris Plus Gel (Fisher Scientific) and the gel was run at 120 V for 75 min. The gel was then removed from the cassette and stained with SimplyBlue SafeStain (Thermo Fisher) for 1 h. The gel was allowed to destain overnight in water, rocking at room temperature before imaging.

To measure the encapsulation efficiency of DOX-loaded PEG-PLGA NPs, 0.5 mg of particles was added to 1 mL of dimethylsulfoxide (DMSO) (Fisher Scientific) and water bath sonicated for 30 min. The amount of DOX in the dissolved NPs was measured by ultraviolet (UV)—visible spectrophotometry (Cary 60 Spectrophotometer, Agilent) where the maximum value between 470 and 490 nm was compared to a standard curve of a known DOX concentration in DMSO.

2.5. Characterization of Drug Loading in PEG-PLGA NPs and MWNPs and the Release of DOX under Storage or Physiologic Conditions. To evaluate the release of DOX from PEG-PLGA NPs and MWNPs, 3 mg of particles was suspended in 1 mL of either storage (water, 4 °C, stationary) or physiological (PBS

pH 5.5 or 7.4, 37 °C, orbital shaker at 100 rpm) conditions. At specified time points (1, 2, 4, 24, and 48 h), the solutions were centrifuged (20,000g, 4 °C, 20 min) and the supernatant containing released DOX was collected. The particles in the pellet were resuspended in fresh solvent and returned to their previous conditions until the next measurement. The supernatant was measured for the presence of DOX by UV—vis spectrophotometry using a Cary60. The maximum value between 470 and 490 nm was compared to a standard curve of a known DOX concentration in the appropriate solvent. After the final measurement, the NP pellet was added to 1 mL of DMSO, and water bath sonicated for 30 min to break down the NPs. The remaining DOX was then measured by UV—vis spectrophotometry and compared to a standard curve in the same volume of DOX in DMSO.

2.6. Imaging of Cellular Uptake of Free DOX, DOX-Loaded PEG-PLGA NPs, and DOX-Loaded MWNPs. To compare DOX uptake by CHRF cells when administered freely or in NP formulations, 4×10^4 CHRF cells was seeded per well of an 8-well chamber plate in PMA-supplemented media for 24 h. Cells were then treated with free DOX, DOX-loaded PEG-PLGA NPs, or DOX-loaded MWNPs at 1.5 μ M. After 4 h of treatment, cells were washed twice with PBS to remove media and excess/non-internalized DOX. Cells were fixed with 4% formaldehyde for 10 min and then washed twice with PBS. Following fixation, the chambers were removed, and a glass cover slip was sealed onto the glass slide for imaging. Images were acquired at 40× magnification on a Zeiss Axioobserver Z1 inverted fluorescence microscope. An increased fluorescent DOX signal was taken to indicate more DOX uptake.

Cellular fluorescence in the images was analyzed using ImageJ. Five background values were captured for each image, and cells were outlined with the freehand selection tool. The area, integrated density, and mean gray value were measured for each selection, and the corrected total cell fluorescence (CTCF) was calculated using the following formula:

 $CTCF = integrated \ density - (area \ of \ selected \ cell$

× mean fluorecence of background)

2.7. Assessment of Cellular Apoptosis and Necrosis Induced by Free DOX, DOX-Loaded PEG-PLGA NPs, and DOX-Loaded MWNPs. Dosing concentrations of 2.5 and 5 $\mu\rm M$ were chosen for studies of cellular apoptosis/necrosis based on an initial Alamar Blue metabolic activity assay performed with increasing (0.78–25 $\mu\rm M$) amounts of DOX-loaded PEG-PLGA NPs (Figure S1). This assay was performed in a 96-well plate with 10,000 cells NPs were added with fresh PMA-supplemented media and allowed to incubate for 48 h. An Alamar Blue Cell Viability Reagent (Thermo Fisher) was then added per the manufacturer's instructions, and cells were further incubated for 4 h in the dark at 37 °C. The signal was assessed on a microplate reader at 570 nm, and data was analyzed compared to a control no-treatment well. Doses were performed in triplicate.

To analyze cell death induced by DOX, 3×10^4 CHRF cells were seeded per well of a 48-well plate in PMA-supplemented media. After 24 h, cells were treated with free DOX, DOX-PEG-PLGA NPs, or DOX-MWNPs at either 2.5 or 5 μ M concentration of DOX, where the free DOX or particles were suspended in PMA-supplemented media. After 24 h of treatment, cell death was assessed by an Annexin V/SYTOX AADvanced stain per the manufacturer's instructions. Briefly, media were removed from the wells, and cells were washed with PBS before Trypsin-EDTA was added to detach cells. Cells were washed twice with PBS and resuspended in 100 μ L of binding buffer. Annexin V (Thermo Fisher) and SYTOX AADvanced Dead Cell Stain (Thermo Fisher) were added, and cells were incubated in the dark at room temperature for 15 min. Samples were analyzed on an Acea NovoCyte 2060 Flow Cytometer using channels for FITC (Annexin V), APC (SYTOX AADvanced), and PE (DOX). Data analysis was performed with NovoExpress software. Density plots using forward scatter and side scatter were used to exclude debris and

create a main cell population gate. Compensation was performed to account for any signal overflow in the channels, and additional gates were based on unstained cells and single-stained controls treated with 1 μ M staurosporine. Analyses presented are the average of three experiments and statistically analyzed by one-way ANOVA with the post hoc Tukey test.

2.8. Evaluating DNA Damage Induced by Free DOX, DOX-Loaded PEG-PLGA NPs, and DOX-Loaded MWNPs. The internal mechanism of cell death induced through DOX delivery was investigated using an H2A.X Phosphorylation Assay Flow Cytometry Kit (Sigma Aldrich). For this assay, 1.5×10^5 CHRF cells were seeded per well in a 12-well plate in PMA-supplemented media. After 24 h, cells were treated with free DOX, DOX-PEG-PLGA NPs, or DOX-MWNPs at a 5 μ M concentration of DOX. After 24 h of treatment, cells were rinsed with PBS and trypsinized. Cells were washed one time in PBS and then fixed, permeabilized, and incubated with either FITC-conjugated anti-phospho H2A.X or normal mouse IgG antibodies per the manufacturer's instructions. Excess antibodies were removed by washing with the kit-provided wash solution, and cells were immediately analyzed by flow cytometry. Density plots using forward scatter and side scatter were used to exclude debris and create a main cell population gate. Data analysis of the FITC signal was performed with NovoExpress software. Experimental results presented are the average of three experiments analyzed by one-way ANOVA with the *post hoc* Tukey test.

3. RESULTS AND DISCUSSION

3.1. Characterization of Membrane-Wrapping and Drug Loading in MWNPs. DOX-loaded PEG-PLGA NPs were synthesized and wrapped in CHRF membranes as depicted in Figure 1A and described in Section 2. CHRF cells, a childhood acute megakaryoblastic leukemia cell line, were used in this work as the membrane source. ^{28,29} A solution containing a ratio of 1:3 PEG-PLGA:PLGA at 2 mg/mL of each polymer was used to formulate NPs that were stirred overnight and purified by centrifugation. Particles were characterized using NTA, TEM, SDS-PAGE, and absorbance measurements. Before membrane wrapping, DOX-loaded PEG-PLGA NPs had a diameter of 123.9 \pm 21.9 nm and a zeta potential of -22.4 ± 4.4 mV (Figure 2A). After wrapping in CHRF membranes, the diameter increased to 137.3 \pm 18.5 nm (Figure 2A), indicative of a 10-20 nm-thick membrane layer present around the particles. The zeta potential of the MWNPs decreased to -29.8 ± 1.9 mV, mirroring that of the CHRF membranes at -30.0 ± 3.6 mV (Figure 2A). Membrane wrapping was also confirmed by SDS-PAGE (Figure 2B) where the complete protein profiles of whole cells, membrane vesicles, and MWNPs can be seen as well as the removed nuclear and mitochondrial fractions during membrane collection. From this, it can be visualized that some bands, notably the strong bands in triplicate below 26 kDa for the nuclear pellet and the band around 50 kDa for the mitochondrial pellet, are reduced or are not present in the membrane vesicle or MWNP lanes. This leads to the conclusion that the nuclear and mitochondrial fractions have been successfully removed during the lysis and centrifugation steps, but future studies would need to corroborate this by additional experimentation such as by Western blotting. Additionally, the comparison of protein between membranes and MWNPs appears to be near identical, showing no major component losses during the wrapping process. To visualize this structure, TEM was performed, showing a lighter ring of membrane coating and a core-shell structure in the MWNP image (Figure 2C).

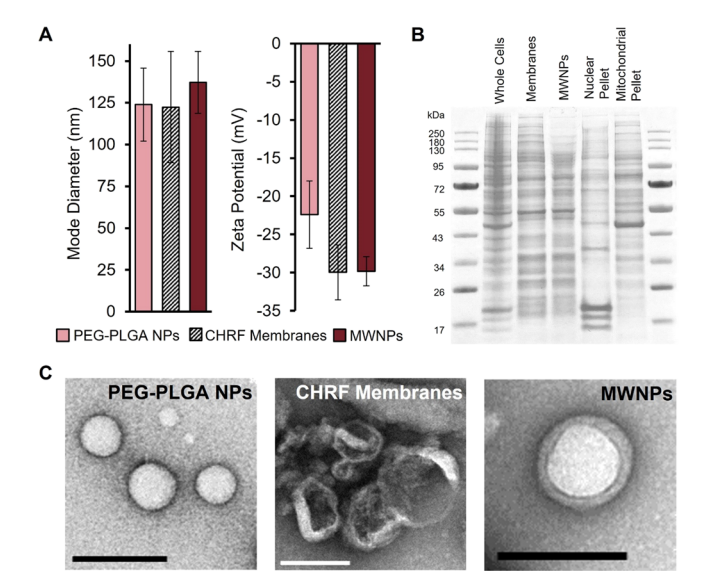


Figure 2. Characterization of MWNPs. (A) The size and charge of PEG-PLGA NPs, extruded CHRF membranes, and MWNPs were measured through Nanoparticle Tracking Analysis and zeta potential (n=3). (B) SDS-PAGE protein profile of whole cells, extruded membranes, MWNPs, and intracellular pellets from membrane collection run at an equal protein concentration. (C) Transmission electron microscopy images of PEG-PLGA NPs, CHRF membranes, and MWNPs. Scale bars = 100 nm.

Following NP synthesis and external characterization, the drug loading and release of PEG-PLGA NPs and MWNPs were investigated. NPs were placed under storage (water, 4 °C) or physiological (PBS at pH 5.5 or 7.4, 37 °C) conditions. The more acidic condition, pH 5.5, is representative of endo/ lysosomal environments and the intracellular conditions of DOX release, whereas the more neutral pH of 7.4 is indicative of bone marrow and circulating blood. 42-45 At 1, 2, 4, 24, and 48 h, NPs were centrifuged to form a pellet and the DOX signal in the supernatant was measured by UV-visible spectrophotometry. The spectrophotometry readings were then compared to a standard curve of DOX in the same solution. After measuring the supernatant, the NP pellets were resuspended in fresh solution and stored until the next time point. At the end of the study (48 h), all final pellets were dissolved in DMSO, and the DOX signal was construed to be the amount of cargo remaining in the NP. Under the storage conditions, PEG-PLGA NPs released 50.8% of their total encapsulated cargo by 48 h, while the MWNPs released 40.0% of the loaded DOX. Cargo release rates were greatly increased under physiologically relevant conditions, with PEG-PLGA NPs at pH 7.4 and 5.5 releasing 88.4 and 97.4% of their cargo by 48 h, respectively. MWNPs in pH 7.4 had a final DOX release of 84.4% with pH 5.5 samples reaching 94.3% (Figure 3A). Overall, when the total released cargo and the amount remaining in the pellet at 48 h were summed, PEG-PLGA NPs encapsulated 14.2 \pm 2.4 μg of DOX per milligram of polymer and MWNPs loaded 5.8 \pm 1.5 μ g of DOX per mg of polymer (Figure 3B; corresponding encapsulation efficiency shown in Figure S2). The reduced loading in MWNPs is likely due to losses during the extrusion process to add the membrane

Taken together, these data indicate the successful synthesis of DOX-loaded PEG-PLGA NPs that can be wrapped in CHRF membranes to form MWNPs. While a decrease in

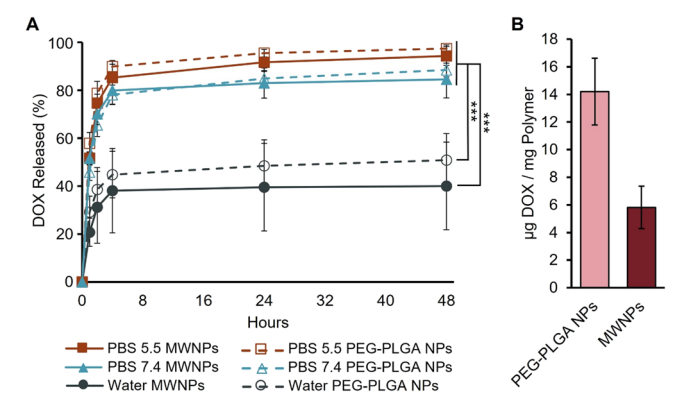


Figure 3. Drug release and loading. (A) DOX release from PEG-PLGA and membrane-wrapped NPs under physiological (37 °C PBS at pH 5.5 or 7.4) and storage (4 °C water) conditions over a 48 h period. (n = 9 for PEG-PLGA NPs, 3 for MWNPs). ***p < 0.0001 calculated by one-way ANOVA with the *post hoc* Tukey test. (B) Loading of DOX in PEG-PLGA NPs and MWNPs. (n = 27 for PEG-PLGA NPs, 9 for MWNPs).

encapsulated cargo is present after membrane wrapping, both formulations release their therapeutic cargo at similar rates under physiological conditions, indicating that the membrane does not hinder timely cargo delivery. Under storage conditions, less than half of the cargo was released from MWNPs, pointing to a potentially beneficial effect of membrane wrapping, halting premature loss before systemic injection.

3.2. MWNPs Improve DOX Delivery into AML Cells. To test the hypothesis that MWNPs would allow for increased DOX delivery into cells owing to improved NP-cell interactions facilitated by the membrane coating, CHRF cells were incubated with free DOX or with DOX-loaded PEG-PLGA NPs or MWNPs. After 4 h, the DOX signal was visualized within cells using fluorescence microscopy (Figure 4A). When quantified in ImageJ, MWNP-treated cells had over 2.4 times more fluorescence than their PEG-PLGA NP counterparts and over 6.3 times more fluorescence than cells exposed to free DOX (Figure 4B). From this, it may be inferred that the MWNPs are able to better target, and deliver cargo to, their homotypic CHRF cells. These data support the hypothesis that the membrane coating maintains its functionality when added to an NP. Additionally, these data suggest that DOX may be more effective when delivered in MWNP formulations owing to the larger amount of DOX that enters the cells. This was tested experimentally as summarized below.

3.3. DOX-Loaded MWNPs Induce Cell Death in Homotypic AML Cells. Following synthesis, characterization, and assessment of cellular interactions, PEG-PLGA NPs and MWNPs were investigated as vehicles to induce leukemic cell death. As it is important to induce apoptosis rather than necrosis for the ideal therapeutic outcome, Annexin V (FITC channel) and SYTOX AAdvanced (APC channel) were used to mark cellular apoptosis and necrosis, respectively. SYTOX AAdvanced was used instead of the more common propidium iodide (PI) agent because PI's excitation/emission spectrum overlaps with the DOX fluorescence spectrum, which could have confounded flow cytometry results. CHRF cells were exposed to 2.5 or 5 μ M of free DOX, DOX-loaded PEG-PLGA NPs, or DOX-loaded MWNPs for 24 h. Cells were then stained with both markers and analyzed via flow cytometry to produce density plots with the Annexin V/FITC channel on

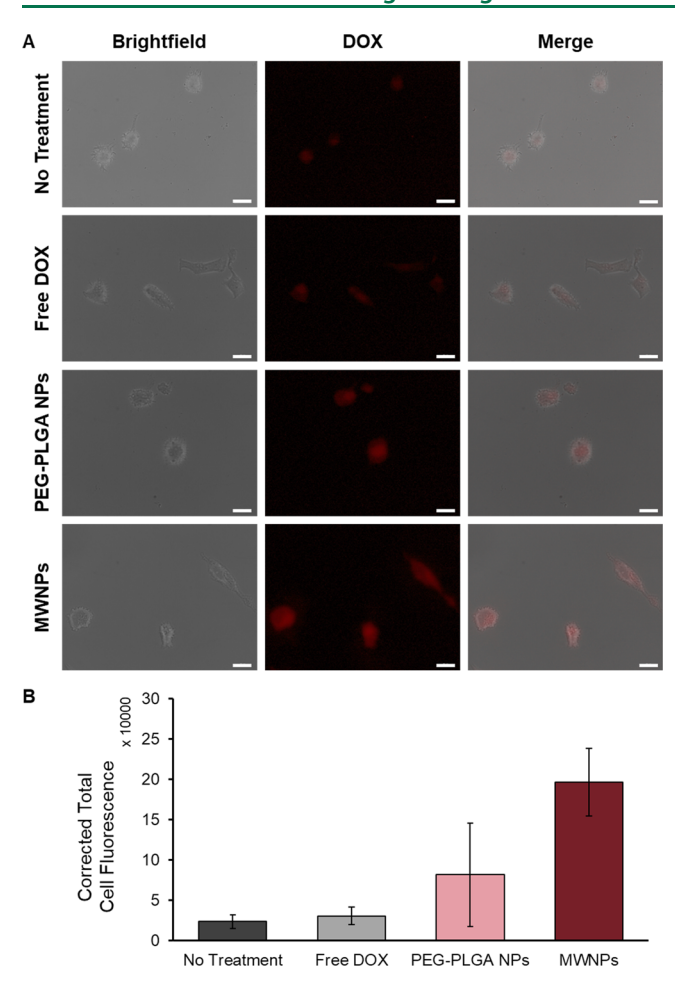


Figure 4. Visualization and quantification of the DOX signal in CHRF cells treated with free DOX, DOX-loaded PEG-PLGA NPs, or DOX-loaded MWNPs. (A) Microscopy images taken at 40× magnification show DOX fluorescence (red) in CHRF cells overlaid with brightfield images. Scale bars = 20 μ m. (B) Quantification of the corrected total cell fluorescence based on the DOX signal from visualized cells as determined in ImageJ.

the x axis and the SYTOX/APC channel on the y axis. Viable cells remain negative for both markers and appear in the bottom left quadrant of the plots. By comparison, cells in early apoptosis are marked by Annexin V only and appear in the bottom right quadrant, cells undergoing late apoptosis are marked by both stains and appear in top right quadrant, and necrotic cells are marked by only SYTOX AADvanced are found in the top left quadrant. The results from this experiment show that both 2.5 and 5.0 µM dosages of DOXloaded MWNPs induce significantly greater levels of apoptosis than the same concentrations of DOX delivered freely or in PEG-PLGA NPs (quantitative data in Figure 5A, with representative flow cytometry plots in Figure 5B). While there was a slight increase in apoptotic cells between the low and high dosages of the free DOX and DOX-PEG-PLGA NPs, all had apoptotic fractions ranging from 12 to 17%. Drastically, the fraction of apoptotic cells in samples treated with MWNPs at 2.5 µM DOX concentrations rose to over 45%, while the 5 μ M dosage yielded approximately 80% apoptosis (Figure 5A). No group had increased levels of necrotic cells, indicating that apoptosis was the predominant mechanism of cell death induced by DOX delivery (Figure S3). These results support the use of MWNPs as potent DOX delivery vehicles.

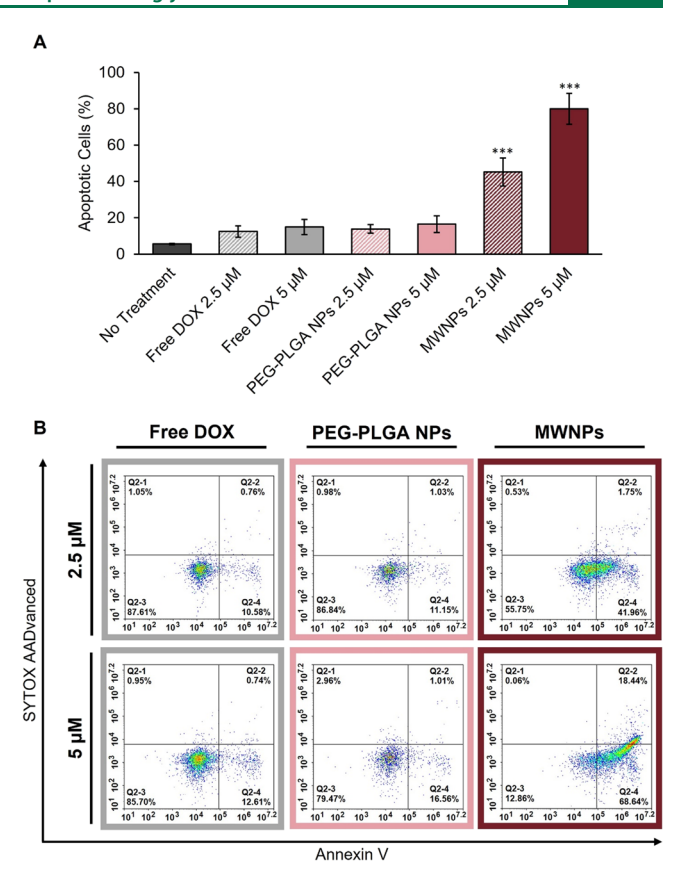


Figure 5. Apoptotic cell death induced by DOX. (A) Percent of cells stained positive for combined early and late apoptosis when treated with either free DOX, PEG-PLGA NPs, or MWNPs at low (2.5 μ M) or high (5 μ M) DOX dosages (n=3). ***p<0.0005 as calculated by one-way ANOVA with the *post hoc* Tukey test. (B) Representative scatterplots demonstrating fraction of cells in early apoptosis (bottom right quadrant), late apoptosis (top right quadrant), or necrosis (top left quadrant) following treatment with free DOX, PEG-PLGA NPs, or MWNPs at DOX concentrations of 2.5 or 5 μ M.

After the mechanism of cell death was confirmed to be primarily apoptotic, an H2A.X phosphorylation assay was carried out to evaluate double-stranded DNA damage that should occur owing to DOX interference with TOP2 (Figure 6A). In this assay, cells are incubated with fluorescent antiphospho-histone H2AX antibodies, and then flow cytometry is performed to quantify the fluorescence signal, which should correlate with the level of DNA damage. We found that CHRF cells treated with DOX either freely, in PEG-PLGA NPs, or in MWNPs had median fluorescence intensities near three times that of the no treatment control (Figure 6B). This indicates that the delivered DOX is functioning as expected to inhibit TOP2 and cause DNA double-strand breaks. Taken in combination with the Annexin V/SYTOX AADvanced experimental data, it may be concluded that MWNPs can induce significantly greater leukemic cell death than control particles and freely delivered drugs and that the mechanistic functionality of delivered DOX is not altered upon entry into the cells.

4. DISCUSSION

This work presents DOX-loaded, membrane-wrapped NPs as promising vehicles for targeted chemotherapeutic delivery to homotypic AML cells. NTA, zeta potential, and TEM analyses

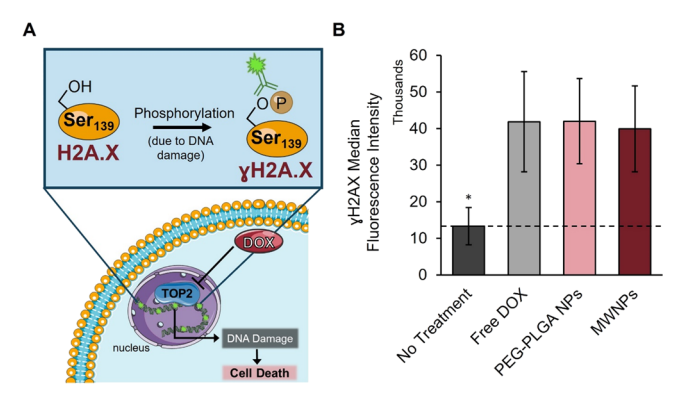


Figure 6. Mechanism of intracellular cell death. (A) Scheme depicting Ser₁₃₉ phosphorylation due to DOX-induced DNA damage. Fluorescent γ H2A.X-specific antibodies specifically bind to the phosphorylated ser-139 residues in the DNA. (B) Flow cytometric analysis of cells treated with 5 μM DOX and incubated with Phospho-Histone H2A.X antibodies. Data represents the median fluorescence intensity of samples, indicative of serine-139 phosphorylation (n = 3). *p < 0.05 as calculated by one-way ANOVA with post-hoc Tukey. Parts of panel A were produced using Servier Medical Art templates. Servier Medical Art by Servier is licensed under a Creative Commons Attribution 3.0 Unported License (https://creativecommons.org/licenses/by/3.0/).

show the successful formation of MWNPs, while SDS-PAGE protein profiles indicate that membrane components are fully transferred onto the NP core while intracellular proteins are removed. The release rate of DOX from both membranewrapped and uncoated PEG-PLGA NPs was explored, and as expected from the thermal stimulus, both systems exhibited faster release over a 48 h time frame when placed under physiologically relevant conditions rather than storage conditions. 46 The release of DOX from the NPs was also pH-dependent. As described by Hines and Kaplan, when water enters the polymer matrix, the hydrolytic degradation of PLGA begins.⁴⁷ As the degradation progresses, the lactic and glycolic acid molecules create a pH gradient, causing increasingly faster swelling and diffusion of the DOX through the autocatalysis of the PLGA. By placing the NPs in a more acidic environment, this process is given a head start, with increased amounts of DOX release observed at more acidic pH levels. 46,47

When administered to CHRF cells in vitro, MWNPs were found to be substantially more efficient and effective than freely delivered DOX or DOX-loaded PEG-PLGA NPs. Almost 50% of cells treated with DOX-loaded MWNPs experienced apoptosis at a dose of 2.5 μ M, which increased to 80% at a higher 5 μ M dose. By comparison, cellular apoptosis ranged between 12 and 17% in samples treated with free DOX or DOX-PEG-PLGA at these doses. This apoptotic cell death is the preferred mechanism of cell death due to its controlled and efficient manner that does not affect the surrounding cells. 48,49 The alternative—uncontrolled, non-regulated necrosis—would induce inflammation through membrane rupture and could release damage-associated molecular patterns that can cause surrounding cells to produce cytokines. 50-,52 Specifically in the bone marrow microenvironment, in addition to causing inflammation, necrosis has been observed to impair normal HSPC function. 52 In the case of AML, HSPCs would have compounded impairment as there is megakaryocyte (Mk) overproduction of $TGF\beta1$, which blocks key functions of HSPCs. These effects may be specifically exaggerated in AML due to the excessive proliferation of immature myeloid precursors, possibly intensifying the effects of $TGF\beta 1$ overproduction. 1,53 Conveniently, one of the functions of DOX in the bone marrow microenvironment is to halt proliferating myeloid cells such as Mks. 54 By using a targeted delivery system to reach these cells, we can combat the excess immature myeloid cells and treat the growing mass of leukemia cells that is crowding out the healthy marrow components. Specific to this work, when the mechanism of cell death was examined by $\gamma H2A.X$ assay, all DOX-treated groups had evidence of intracellular DNA damage, indicating no functional change in the DOX's mechanism of action following release from the NPs. Taken together, these studies along with the fluorescence microscopy studies indicate MWNPs are a robust drug delivery system with great potential for future exploration.

Future directions for this work could tune and slow the release rate of DOX from the NPs by increasing the polymer concentration during synthesis and then examine how release kinetics impact therapeutic efficacy. Papers have shown that by using PLGA at a concentration of 25 mg/mL, instead of the 2 mg/mL used in this work, the release of DOX from the NP can be extended over 14 days.⁵⁵ Our NPs exhibit rapid DOX release within the first 4 h of exposure to physiological conditions (Figure 3). This is due to the phenomenon of burst release, a common concern when using loaded PLGA. 56 While higher drug loading can contribute to this initial release due to the drug:polymer concentration, it is also attributed to the adsorbed drug on the surface of the NPs. 57,58 To ensure that sufficient cargo reaches cells in the blood and bone marrow (rather than being released prematurely in circulation), the polymer composition could be tuned. For example, by changing the polymer molecular weight or increasing its density, it may be possible to improve drug loading and minimize burst release such that most of the cargo is released after 4-12 h of circulation, allowing the particles time to accumulate at their target site. In addition to tuning the core of the NPs, the shell should also be considered. A potential limitation of this study is that we do not know the precise fraction of NPs in each sample that is fully coated, partially coated, or uncoated. As recent work has indicated that the completeness of membrane-wrapping can impact MWNP performance, the future work should aim to determine the fraction of fully/partially/unwrapped NPs in the sample and achieve complete membrane wrapping.⁵⁹ Lastly, another area of consideration regarding NP synthesis is to find a way to lessen the cargo drop between unwrapped NPs and MWNPs. To address this, experiments could be performed reducing the number of extrusions the membranes and NPs are subject to for wrapping or increasing the amount of initially loaded drug to account for this loss.

As mentioned earlier, clinical dosing with anthracyclines, including DOX, often occurs alongside delivery of cytarabines, specifically in a 7 + 3 plan where cytarabine is infused over 7 treatment days, with overlapping anthracycline dosing occurring only on the first 3 days. Significant knowledge could be gained from performing studies that introduce cytarabines, or other molecules, into the particle system, whether co-encapsulated in the same NP or delivered in separate particles. Furthering this idea, a dosing regimen for *in vivo* experiments would need to be designed for treatment of AML and other leukemia/blood disorders, depending on the release rate of the cargo(s). These experiments could involve

additional studies comparing the efficacy and safety to DOXIL or similar liposomal formulations that are clinically used.

Related to the future *in vivo* work, it will be important to carefully select an appropriate animal model for preclinical validation studies. As the membranes used to produce MWNPs in this work are derived from human cells, it would be best to perform animal studies in humanized mice so that the efficacy and safety of the system can be accurately and robustly characterized. A previous work has shown that murine AML MWNPs are effective in C57BL/6J mice, but studies of human AML MWNPs in mice remain to be performed. ¹⁵ Such experiments will be an important step in the translation of this type of technology from the laboratory to the clinic.

5. CONCLUSIONS

Overall, this work demonstrates that DOX-loaded MWNPs can be successfully synthesized, characterized, and deployed as potent drug delivery vehicles. These AML MWNPs effectively deliver their cargo to homotypic cells to induce apoptosis at substantially higher rates than freely delivered DOX or nontargeted, DOX-loaded, PEG-PLGA NPs. With additional development and investigation, MWNPs may drastically improve the patient experience during chemotherapy treatment by providing a safer, more effective, targeted delivery system.

ASSOCIATED CONTENT

Supporting Information

The Supporting Information is available free of charge at https://pubs.acs.org/doi/10.1021/acsbiomaterials.2c00832.

Alamar Blue assay for dosing concentration, encapsulation efficiency of PEG-PLGA NPs and MWNPs, and full cell death staining profile (PDF)

AUTHOR INFORMATION

Corresponding Author

Emily S. Day — Department of Materials Science and Engineering, University of Delaware, Newark, Delaware 19716, United States; Department of Biomedical Engineering, University of Delaware, Newark, Delaware 19713, United States; Helen F. Graham Cancer Center and Research Institute, Newark, Delaware 19713, United States; orcid.org/0000-0002-8707-826X; Email: emilyday@udel.edu

Authors

Jenna C. Harris – Department of Materials Science and Engineering, University of Delaware, Newark, Delaware 19716, United States

Eric H. Sterin – Department of Biomedical Engineering, University of Delaware, Newark, Delaware 19713, United States; orcid.org/0000-0002-4705-5717

Complete contact information is available at: https://pubs.acs.org/10.1021/acsbiomaterials.2c00832

Author Contributions

The project was funded through work by E.S.D. Experiments and data analysis were performed by J.C.H. The microscopy work was performed by E.H.S. The manuscript was written by J.C.H. and E.S.D. All authors have given approval to the final version of the manuscript.

Funding

Funding was provided by a University City Science Center QED Grant, by the National Science Foundation (NSF) under CAREER Award DMR1752009, and by the National Institutes of Health under award numbers R35GM119659 and U54GM104941. This material is based upon work supported by the NSF Graduate Research Fellowship Program under grant no. 1940700. Any opinions, findings, and conclusions or recommendations expressed in this material are those of the author(s) and do not necessarily reflect the views of the funding agencies.

Notes

The authors declare the following competing financial interest(s): The authors have a patent pending related to the MWNP technology under international PCT application number PCT/US2019/063685.

ACKNOWLEDGMENTS

Electron microscopy access was supported by grants from the National Institutes of Health-National Institute of General Medical Sciences (P20 GM103446 and P20GM139760) and the State of Delaware.

ABBREVIATIONS

MWNP, membrane-wrapped nanoparticle; NP, nanoparticle; AML, acute myeloid leukemia; DOX, doxorubicin; ROS, reactive oxygen species; HSPCs, hematopoietic stem and progenitor cells; CHRF, CHRF-288-11; TOP2, topoisomerase-II; Mk, megakaryocyte; PEG-PLGA, poly(ethylene glycol)-poly(lactic-co-glycolic acid); MWCO, molecular weight cutoff; NTA, nanoparticle tracking analysis; TEM, transmission electron microscopy; DC, detergent compatible; DMSO, dimethylsulfoxide; UV, ultraviolet; CTCF, corrected total cell fluorescence; SDS-PAGE, sodium dodecyl-sulfate polyacrylamide gel electrophoresis; PI, propidium iodide

■ REFERENCES

- (1) Jäger, P.; Geyh, S.; Twarock, S.; Cadeddu, R. P.; Rabes, P.; Koch, A.; Maus, U.; Hesper, T.; Zilkens, C.; Rautenberg, C.; Bormann, F.; Köhrer, K.; Petzsch, P.; Wieczorek, D.; Betz, B.; Surowy, H.; Hildebrandt, B.; Germing, U.; Kobbe, G.; Haas, R.; Schroeder, T. Acute Myeloid Leukemia-Induced Functional Inhibition of Healthy CD34+ Hematopoietic Stem and Progenitor Cells. *Stem Cells* **2021**, 39, 1270–1284.
- (2) de Rooij, J. D.; Zwaan, C. M.; van den Heuvel-Eibrink, M. Pediatric AML: From Biology to Clinical Management. *J. Clin. Med.* **2015**, *4*, 127.
- (3) Kantarjian, H.; Kadia, T.; DiNardo, C.; Daver, N.; Borthakur, G.; Jabbour, E.; Garcia-Manero, G.; Konopleva, M.; Ravandi, F. Acute Myeloid Leukemia: Current Progress and Future Directions. *Blood Cancer J.* **2021**, *11*, 41.
- (4) Zeidan, A. M.; Podoltsev, N. A.; Wang, X.; Zhang, C.; Bewersdorf, J. P.; Shallis, R. M.; Huntington, S. F.; Neparidze, N.; Giri, S.; Gore, S. D.; Davidoff, A. J.; Ma, X.; Wang, R. Patterns of Care and Clinical Outcomes with Cytarabine-Anthracycline Induction Chemotherapy for AML Patients in the United States. *Blood Adv.* **2020**, *4*, 1615–1623.
- (5) Pasvolsky, O.; Morelli, O.; Rozovski, U.; Vaturi, M.; Wolach, O.; Amitai, I.; Vaxman, I.; Ratzon, R.; Yeshurun, M.; Kornowski, R.; Iakobishvilli, Z.; Raanani, P. Anthracycline-Induced Cardiotoxicity in Acute Myeloid Leukemia Patients Who Undergo Allogeneic Hematopoietic Stem Cell Transplantation. *Clin. Lymphoma Myeloma Leuk.* 2019, 19, e343—e348.

- (6) Acute myeloid leukaemia Treatment NHS. https://www.nhs.uk/conditions/acute-myeloid-leukaemia/treatment/ (accessed 2022-05-09).
- (7) Magina, K. N.; Pregartner, G.; Zebisch, A.; Wölfler, A.; Neumeister, P.; Greinix, H. T.; Berghold, A.; Sill, H. Cytarabine Dose in the Consolidation Treatment of AML: A Systematic Review and Meta-Analysis. *Blood* **2017**, *130*, 946–948.
- (8) Appelbaum, F. R.; Bernstein, I. D. Gemtuzumab Ozogamicin for Acute Myeloid Leukemia. *Blood* **2017**, *130*, 2373–2376.
- (9) Vollmar, B. S.; Frantz, C.; Schutten, M. M.; Zhong, F.; del Rosario, G.; Go, M. A. T.; Yu, S. F.; Leipold, D. D.; Kamath, A. V.; Ng, C.; Xu, K.; dela Cruz-Chuh, J.; Kozak, K. R.; Chen, J.; Xu, Z.; Wai, J.; Adhikari, P.; Erickson, H. K.; Dragovich, P. S.; Polson, A. G.; Pillow, T. H. Calicheamicin Antibody-Drug Conjugates with Improved Properties. *Mol. Cancer Ther.* **2021**, *20*, 1112–1120.
- (10) Ci, T.; Li, H.; Chen, G.; Wang, Z.; Wang, J.; Abdou, P.; Tu, Y.; Dotti, G.; Gu, Z. Cryo-Shocked Cancer Cells for Targeted Drug Delivery and Vaccination. *Sci. Adv.* **2020**, *6*, No. eabc3013.
- (11) Harris, J. C.; Scully, M. A.; Day, E. S. Cancer Cell Membrane-Coated Nanoparticles for Cancer Management. *Cancers* **2019**, *11*, 1836
- (12) Xu, L.; Wu, S.; Wang, J. Cancer Cell Membrane—Coated Nanocarriers for Homologous Target Inhibiting the Growth of Hepatocellular Carcinoma. *J. Bioact. Compat. Polym.* **2019**, 34, 58—71.
- (13) Jiang, Q.; Liu, Y.; Guo, R.; Yao, X.; Sung, S.; Pang, Z.; Yang, W. Erythrocyte-Cancer Hybrid Membrane-Camouflaged Melanin Nanoparticles for Enhancing Photothermal Therapy Efficacy in Tumors. *Biomaterials* **2019**, *192*, 292–308.
- (14) Wang, P.; Kankala, R. K.; Chen, B.; Zhang, Y.; Zhu, M.; Li, X.; Long, R.; Yang, D.; Krastev, R.; Wang, S.; Xiong, X.; Liu, Y. Cancer Cytomembrane-Cloaked Prussian Blue Nanoparticles Enhance the Efficacy of Mild-Temperature Photothermal Therapy by Disrupting Mitochondrial Functions of Cancer Cells. ACS Appl. Mater. Interfaces 2021, 13, 37563–37577.
- (15) Johnson, D. T.; Zhou, J.; Kroll, A. V.; Fang, R. H.; Yan, M.; Xiao, C.; Chen, X.; Kline, J.; Zhang, L.; Zhang, D. E. Acute Myeloid Leukemia Cell Membrane-Coated Nanoparticles for Cancer Vaccination Immunotherapy. 2022, 994, DOI: 10.1038/s41375-021-01432-w.
- (16) Russkamp, N. F.; Myburgh, R.; Kiefer, J. D.; Neri, D.; Manz, M. G. Anti-CD117 Immunotherapy to Eliminate Hematopoietic and Leukemia Stem Cells. *Exp. Hematol.* **2021**, *95*, 31–45.
- (17) McClendon, A. K.; Osheroff, N. DNA Topoisomerase II, Genotoxicity, and Cancer. *Mutat. Res.* **2007**, 623, 897.
- (18) Nitiss, J. L. DNA Topoisomerase II and Its Growing Repertoire of Biological Functions. *Nat. Rev. Cancer* **2009**, *9*, 327–337.
- (19) Wenningmann, N.; Knapp, M.; Ande, A.; Vaidya, T. R.; Ait-Oudhia, S. Insights into Doxorubicin-Induced Cardiotoxicity: Molecular Mechanisms, Preventive Strategies, and Early Monitoring. *Mol. Pharmacol.* **2019**, *96*, 219–232.
- (20) Kim, H. S.; Lee, Y. S.; Kim, D. K. Doxorubicin Exerts Cytotoxic Effects through Cell Cycle Arrest and Fas-Mediated Cell Death. *Pharmacology* **2009**, *84*, 300–309.
- (21) Mah, L. J.; El-Osta, A.; Karagiannis, T. C. ΓH2AX: A Sensitive Molecular Marker of DNA Damage and Repair. *Leukemia* **2010**, *24*, 679–686.
- (22) Eom, Y. W.; Kim, M. A.; Park, S. S.; Goo, M. J.; Kwon, H. J.; Sohn, S.; Kim, W. H.; Yoon, G.; Choi, K. S. Two Distinct Modes of Cell Death Induced by Doxorubicin: Apoptosis and Cell Death through Mitotic Catastrophe Accompanied by Senescence-like Phenotype. *Oncogene* **2005**, 24, 4765–4777.
- (23) He, H.; Wang, L.; Qiao, Y.; Zhou, Q.; Li, H.; Chen, S.; Yin, D.; Huang, Q.; He, M. Doxorubicin Induces Endotheliotoxicity and Mitochondrial Dysfunction via ROS/ENOS/NO Pathway. *Front. Pharmacol.* **2019**, *10*, 1–16.
- (24) Gammella, E.; Maccarinelli, F.; Buratti, P.; Recalcati, S.; Cairo, G. The Role of Iron in Anthracycline Cardiotoxicity. *Front. Pharmacol* **2014**, *5*, 1–6.

- (25) Yang, R.; Li, Y.; Wang, X.; Yan, J.; Pan, D.; Xu, Y.; Wang, L.; Yang, M. Doxorubicin Loaded Ferritin Nanoparticles for Ferroptosis Enhanced Targeted Killing of Cancer Cells. *RSC Adv.* **2019**, *9*, 28548–28553.
- (26) Zhao, L.; Zhang, B. Doxorubicin Induces Cardiotoxicity through Upregulation of Death Receptors Mediated Apoptosis in Cardiomyocytes. *Sci. Rep.* **2017**, *7*, 1–11.
- (27) Escobar, C.; Kao, C. Y.; Das, S.; Papoutsakis, E. T. Human Megakaryocytic Microparticles Induce de Novo Platelet Biogenesis in a Wild-Type Murine Model. *Blood Adv.* **2020**, *4*, 804–814.
- (28) Fuhrken, P. G.; Chen, C.; Miller, W. M.; Papoutsakis, E. T. Comparative, Genome-Scale Transcriptional Analysis of CHRF-288-11 and Primary Human Megakaryocytic Cell Cultures Provides Novel Insights into Lineage-Specific Differentiation. *Exp. Hematol.* **2007**, *35*, 476–489.e23.
- (29) Kao, C. Y.; Papoutsakis, E. T. Engineering Human Megakaryocytic Microparticles for Targeted Delivery of Nucleic Acids to Hematopoietic Stem and Progenitor Cells. *Sci. Adv.* **2018**, *4*, No. eaau6762.
- (30) Wells, S. J.; Bray, R. A.; Stempora, L. L.; Farhi, D. C. CD117/CD34 Expression in Leukemic Blasts. *Am. J. Clin. Pathol.* 1996, 106, 192–195.
- (31) Ahmadi, A.; Poorfathollah, A. A.; Aghaiipour, M.; Rezaei, M.; Nikoo-Ghoftar, M.; Abdi, M.; Gharib, A.; Amini, A. Diagnostic Value of CD117 in Differential Diagnosis of Acute Leukemias. *Tumor Biol.* **2014**, *35*, 6763–6768.
- (32) Rassidakis, G. Z.; Georgakis, G. V.; Oyarzo, M.; Younes, A.; Medeiros, L. J. Lack of C-Kit (CD117) Expression in CD30+Lymphomas and Lymphomatoid Papulosis. *Mod. Pathol.* **2004**, *17*, 946–953.
- (33) Cascavilla, N.; Musto, P.; D'Arena, G.; Melillo, L.; Carella, A. M.; Petrilli, M. P.; Sanpaolo, G.; Carotenuto, M. CD117 (c-Kit) Is a Restricted Antigen of Acute Myeloid Leukemia and Characterizes Early Differentiative Levels of M5 FAB Subtype. *Haematologica* **1998**, 83, 392–397.
- (34) Escribano, L.; Ocqueteaub, M.; Almeida, J.; Orfao, A.; Migue, J. F. S. Expression of the C-Kit (CD117) Molecule in Normal and Malignant Hematopoiesis. *Leuk. Lymphoma* **1998**, *30*, 459–466.
- (35) Czechowicz, A.; Palchaudhuri, R.; Scheck, A.; Hu, Y.; Hoggatt, J.; Saez, B.; Pang, W. W.; Mansour, M. K.; Tate, T. A.; Chan, Y. Y.; Walck, E.; Wernig, G.; Shizuru, J. A.; Winau, F.; Scadden, D. T.; Rossi, D. J. Selective Hematopoietic Stem Cell Ablation Using CD117-Antibody-Drug-Conjugates Enables Safe and Effective Transplantation with Immunity Preservation. *Nat. Commun.* 2019, 10, 1–12
- (36) Fang, R. H.; Hu, C.-M. M. J.; Luk, B. T.; Gao, W.; Copp, J. A.; Tai, Y.; O'Connor, D. E.; Zhang, L.; O'Connor, D. E.; Zhang, L.; O'Connor, D. E.; Zhang, L. Cancer Cell Membrane-Coated Nanoparticles for Anticancer Vaccination and Drug Delivery. *Nano Lett.* 2014, 14, 2181–2188.
- (37) Rosca, I. D.; Watari, F.; Uo, M. Microparticle Formation and Its Mechanism in Single and Double Emulsion Solvent Evaporation. *J. Controlled Release* **2004**, *99*, 271–280.
- (38) McCall, R. L.; Sirianni, R. W. PLGA Nanoparticles Formed by Single- or Double-Emulsion with Vitamin E-TPGS. *J. Visualized Exp.* **2013**, *82*, 1–8.
- (39) Astete, C. E.; Sabliov, C. M. Synthesis and Characterization of PLGA Nanoparticles. *J. Biomater. Sci. Polym. Ed.* **2006**, 17, 247–289.
- (40) Gholizadeh, S.; Kamps, J. A. A. M.; Hennink, W. E.; Kok, R. J. PLGA-PEG Nanoparticles for Targeted Delivery of the MTOR/PI3kinase Inhibitor Dactolisib to Inflamed Endothelium. *Int. J. Pharm.* **2018**, *548*, 747–758.
- (41) Bachurski, D.; Schuldner, M.; Nguyen, P. H.; Malz, A.; Reiners, K. S.; Grenzi, P. C.; Babatz, F.; Schauss, A. C.; Hansen, H. P.; Hallek, M.; Pogge von Strandmann, E. Extracellular Vesicle Measurements with Nanoparticle Tracking Analysis—An Accuracy and Repeatability Comparison between NanoSight NS300 and ZetaView. *J. Extracell. Vesicles* 2019, 8, 1596016.

- (42) Hu, Y. B.; Dammer, E. B.; Ren, R. J.; Wang, G. The Endosomal-Lysosomal System: From Acidification and Cargo Sorting to Neurodegeneration. *Transl. Neurodegener.* **2015**, *4*, 1–10.
- (43) Nikolaeva, L. P. Features of Acid Base Balance of Bone Marrow. *Acta Medica Int.* **2018**, *5*, 55–57.
- (44) Yeh, S. A.; Hou, J.; Wu, J. W.; Yu, S.; Zhang, Y.; Belfield, K. D.; Camargo, F. D.; Lin, C. P. Quantification of Bone Marrow Interstitial PH and Calcium Concentration by Intravital Ratiometric Imaging. *Nat. Commun.* **2022**, *13*, 1–13.
- (45) Miettinen, J. A.; Salonen, R. J.; Ylitalo, K.; Niemelä, M.; Kervinen, K.; Säily, M.; Koistinen, P.; Savolainen, E. R.; Mäkikallio, T. H.; Huikuri, H. V.; Lehenkari, P. The Effect of Bone Marrow Microenvironment on the Functional Properties of the Therapeutic Bone Marrow-Derived Cells in Patients with Acute Myocardial Infarction. *J. Transl. Med.* **2012**, *10*, 1–11.
- (46) Pillai, O.; Panchagnula, R. Polymers in Drug Delivery. Curr. Opin. Chem. Biol. 2001, 5, 447–451.
- (47) Hines, D. J.; Kaplan, D. L. Poly (Lactic-Co-Glycolic Acid) Controlled Release Systems: Experimental and Modeling Insights. *Crit. Rev. Ther. Drug Carrier Syst.* **2013**, *30*, 257.
- (48) Elmore, S. Apoptosis: A Review of Programmed Cell Death. *Toxicol. Pathol.* **2007**, *35*, 495–516.
- (49) Taylor, R. C.; Cullen, S. P.; Martin, S. J. Apoptosis: Controlled Demolition at the Cellular Level. *Nat. Rev. Mol. Cell Biol.* **2008**, *9*, 231–241.
- (50) Belizário, J.; Vieira-Cordeiro, L.; Enns, S. Necroptotic Cell Death Signaling and Execution Pathway: Lessons from Knockout Mice. *Mediators Inflamm.* **2015**, 2015, 1.
- (51) Yan, G.; Elbadawi, M.; Efferth, T. Multiple Cell Death Modalities and Their Key Features (Review). *World Acad. Sci. J.* **2020**, 2, 39–48.
- (52) Wagner, P. N.; Shi, Q.; Salisbury-Ruf, C. T.; Zou, J.; Savona, M. R.; Fedoriw, Y.; Zinkel, S. S. Increased Ripk1-Mediated Bone Marrow Necroptosis Leads to Myelodysplasia and Bone Marrow Failure in Mice. *Blood* **2019**, *133*, 107–120.
- (53) Gong, Y.; Zhao, M.; Yang, W.; Gao, A.; Yin, X.; Hu, L.; Wang, X.; Xu, J.; Hao, S.; Cheng, T.; Cheng, H. Megakaryocyte-Derived Excessive Transforming Growth Factor B1 Inhibits Proliferation of Normal Hematopoietic Stem Cells in Acute Myeloid Leukemia. *Exp. Hematol.* **2018**, *60*, 40–46.e2.
- (54) Pfizer. PRODUCT INFORMATION ADRIAMYCIN CS Doxorubicin Hydrochloride; 2020.
- (55) Kim, J.; Choi, Y.; Yang, S.; Lee, J.; Choi, J.; Moon, Y.; Kim, J.; Shim, N.; Cho, H.; Shim, M. K.; Jeon, S.; Lim, D. K.; Yoon, H. Y.; Kim, K. Sustained and Long-Term Release of Doxorubicin from PLGA Nanoparticles for Eliciting Anti-Tumor Immune Responses. *Pharmaceutics* **2022**, *14*, 1–17.
- (56) Cruz, L. J.; van Dijk, T.; Vepris, O.; Li, T. M. W. Y.; Schomann, T.; Baldazzi, F.; Kurita, R.; Nakamura, Y.; Grosveld, F.; Philipsen, S.; Eich, C. PLGA-Nanoparticles for Intracellular Delivery of the CRISPR-Complex to Elevate Fetal Globin Expression in Erythroid Cells. *Biomaterials* **2021**, *268*, No. 120580.
- (57) Makadia, H. K.; Siegel, S. J. Poly Lactic-Co-Glycolic Acid (PLGA) as Biodegradable Controlled Drug Delivery Carrier. *Polymer* **2011**, *3*, 1377–1397.
- (58) Danhier, F.; Ansorena, E.; Silva, J. M.; Coco, R.; Le Breton, A.; Préat, V. PLGA-Based Nanoparticles: An Overview of Biomedical Applications. *J. Controlled Release* **2012**, *161*, 505–522.
- (59) Liu, L.; Bai, X.; Martikainen, M. V.; Kårlund, A.; Roponen, M.; Xu, W.; Hu, G.; Tasciotti, E.; Lehto, V. P. Cell Membrane Coating Integrity Affects the Internalization Mechanism of Biomimetic Nanoparticles. *Nat. Commun.* **2021**, *12*, 1–12.